

Mechanistic Studies of the TRIP Catalyzed Allylation with Organozinc Reagents

Peter E. Hartmann, Mattia Lazzarotto, Jakob Pletz, Stefan Tanda, Philipp Neu, Walter Goessler, Wolfgang Kroutil, A. Daniel Boese, and Michael Fuchs

J. Org. Chem., **Just Accepted Manuscript** • DOI: 10.1021/acs.joc.0c00992 • Publication Date (Web): 10 Jul 2020

Downloaded from pubs.acs.org on July 13, 2020

Just Accepted

“Just Accepted” manuscripts have been peer-reviewed and accepted for publication. They are posted online prior to technical editing, formatting for publication and author proofing. The American Chemical Society provides “Just Accepted” as a service to the research community to expedite the dissemination of scientific material as soon as possible after acceptance. “Just Accepted” manuscripts appear in full in PDF format accompanied by an HTML abstract. “Just Accepted” manuscripts have been fully peer reviewed, but should not be considered the official version of record. They are citable by the Digital Object Identifier (DOI®). “Just Accepted” is an optional service offered to authors. Therefore, the “Just Accepted” Web site may not include all articles that will be published in the journal. After a manuscript is technically edited and formatted, it will be removed from the “Just Accepted” Web site and published as an ASAP article. Note that technical editing may introduce minor changes to the manuscript text and/or graphics which could affect content, and all legal disclaimers and ethical guidelines that apply to the journal pertain. ACS cannot be held responsible for errors or consequences arising from the use of information contained in these “Just Accepted” manuscripts.

Mechanistic Studies of the TRIP Catalyzed Allylation with Organozinc Reagents

Peter E. Hartmann,^{†,‡} Mattia Lazzarotto,[†] Jakob Pletz,[†] Stefan Tanda,[§] Philipp Neu,[†] Walter Goessler,[§] Wolfgang Kroutil,[†] A. Daniel Boese,^{‡,*} Michael Fuchs^{†,*}

[†] University of Graz, Institute of Chemistry, Bioorganic and Organic Chemistry, Heinrichstrasse 28/II, 8010 Graz, Austria, Europe.

[‡] University of Graz, Institute of Chemistry, Physical and Theoretical Chemistry, Heinrichstrasse 28/IV, 8010 Graz, Austria, Europe.

[§] University of Graz, Institute of Chemistry, Analytical Chemistry, Universitätsplatz 1/I, 8010 Graz, Austria, Europe.

Keywords: Chiral Phosphoric Acids, Asymmetric Allylation, Ab Initio Calculations, Reaction Mechanisms, Organocatalysis

ABSTRACT: 3,3-Bis(2,4,6-triisopropylphenyl)-1,1-binaphthyl-2,2-diyl hydrogenphosphate (TRIP) catalyzes the asymmetric allylation of aldehydes with organozinc compounds leading to highly valuable structural motifs, like precursors to lignan natural products. Our mechanistic proposal previously reported relies on two reaction intermediates and requires further investigation in order to really understand the mode of action and the origins of stereoselectivity. Detailed *ab initio* calculations, supported by experimental data, render a substantially different mode of action to the allyl boronate congener. Instead of a Brønsted acid based catalytic activation, the chiral phosphate acts as a counterion for the Lewis acidic zinc ion, which provides the activation of the aldehyde.

Introduction

Computational efforts have become a frequent tool in the elucidation of mechanistic scenarios and understanding the course of chemical reactions.¹⁻³ They allow the evaluation of different events by the comparison of their energetic profiles and deliver useful information in order to understand and improve the chemistry behind the process of interest.¹⁻⁴ Especially in combination with asymmetric synthesis, density functional theory (DFT) calculations have facilitated the finding of asymmetric induction and have delivered or confirmed the accepted mechanistic concept of activation and stereopreference. Regarding asymmetric synthesis, allylation reactions have a pronounced foundation and are an indispensable methodology when it comes to the creation of chiral molecules.⁵⁻¹⁰ One of these examples is the asymmetric preparation of dibenzylbutyrolactones, which proceeds via the asymmetric allylation of an aldehyde precursor with an organozinc reagent.¹¹⁻¹² The catalyst – namely 3,3-bis(2,4,6-triisopropylphenyl)-1,1-binaphthyl-2,2-diyl hydrogenphosphate (TRIP, **2**)¹³ – shows high stereoselectivity on the process and delivers the natural product precursor with an enantiomeric excess as high as 98%. Important to note is the fact, that the reaction has a boron congener, using allyl boronate reagents and the same catalyst.¹⁴ Some effort has been undertaken to explain the stereoselectivity in case of these reagents, and yielded a mechanistic mode of action as depicted in Figure 1.¹⁵⁻¹⁷ The decrease of the activation barrier is explained by the hydrogen bond to the pinacol oxygen, activating the

reagent, whereas the required rigidity for the alignment is reasoned by a formyl-H interaction with the P=O oxygen Lewis base.

For the zinc-based reaction, the absence of the pinacol system renders this activation impossible, and our initial mechanistic proposal was based on the energetical assessment of two reaction intermediates. Therefore, additional investigations are required to understand the differences of these allylation reactions.

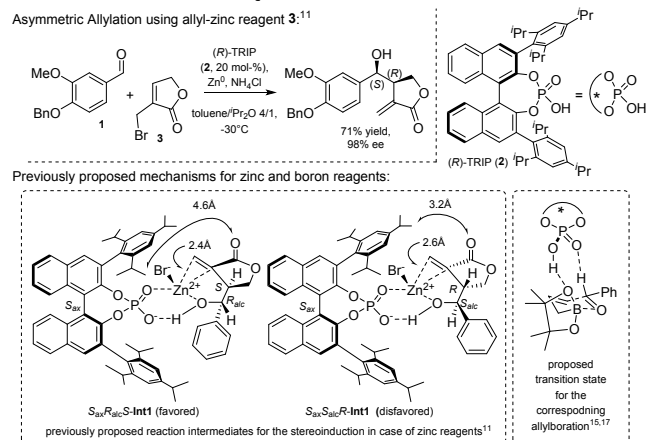


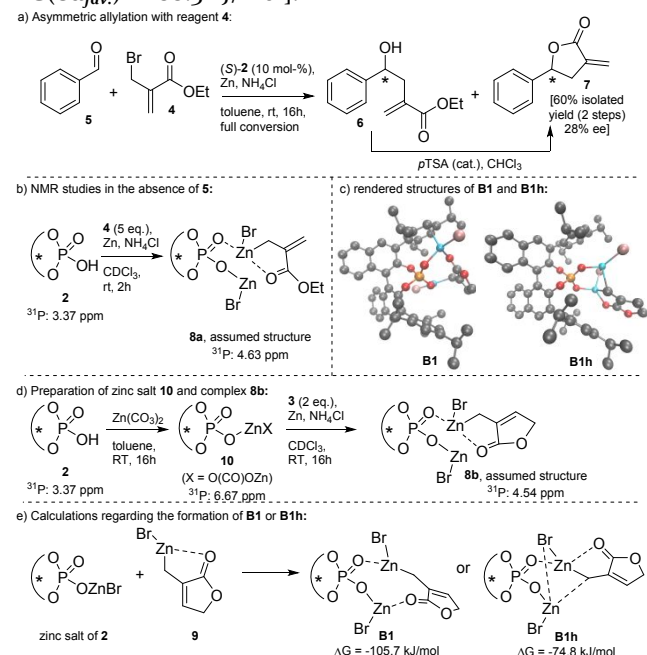
Figure 1. Asymmetric allylation of aldehydes with bromolactone **3** and previously reported rationales for the reactivity and the stereoselectivity of catalyst **2** for the zinc- and boron-based reagents.

Results and Discussion

In order to investigate the reactivity of the TRIP acid (**2**)

under reaction conditions, we probed the acid in the presence of compound **3** and zinc dust (see Scheme 1). The NMR spectra show strong peak broadening due to the unfavorable properties of the NMR-active zinc. The resolution of the recorded spectra slightly improves when the allylic bromide was changed to compound **4** (see Scheme 1a). The reaction with this open-chain, allylic bromide (**4**) yields the allylated product **6** under TRIP catalysis too, albeit with significantly reduced stereoselectivity [99% conv., 60% isolated yield for product **7** (over 2 steps), 28% ee, see Scheme 1a]. Alternatively, the initially envisaged complex **8b** was prepared via the preformed zinc salt **10** and its subjection to the in-situ formed reagent **9** (see Scheme 1d). The observed shift in the ^{31}P NMR spectrum is in almost perfect agreement with the one observed for complex **8a** – a reasonable observation due to their highly similar environment for the zinc core [4.63 ppm (**8a**) and 4.54 ppm (**8b**)]. The formation of a zinc phosphate salt under reaction conditions finds additional support in the detection of protodemetalated reagent **9** via headspace GC-MS analysis. Whereas only little amounts of the quenched reagent **9** form in the absence of TRIP (presumably via a quench by the ammonium salt), significantly higher amounts were detected in the presence of the chiral phosphoric acid reflecting the 20 mol-% used in the experiment (for details see experimental section and supporting information, chapter 2.5).

Scheme 1. a) asymmetric allylation with reagent **4** and b) ^{31}P -NMR studies of the catalyst under reaction conditions in the absence of benzaldehyde (**5**); c) rendered structures of the most stable conformers **B1** and **B1h**;¹⁸ d) preparation of zinc salt **10** and complex **8b**; e) calculations of the quench and coordination of TRIP (**2**) and reagent **9** at the DLPNO-CCSD(T)/cc-pVTZ $\Delta\text{G}+\text{COSMO}$ level [compare to $\Delta\text{G}(\text{ed}_{\text{fav.}}) = -88.3$ kJ/mol].



This observed quench of **2** by zinc organyls has even precedence in literature and has been documented even by a crystal structure of a homologue phosphate.¹⁹ Important to note is that within the homologue zinc complex, both oxygen atoms of the phosphate interact with the zinc species forming a dimeric zinc salt – a fact that our calculations suggest for the outlined transition states herein too (vide infra).¹⁹ Finally, the question remained which complexes of the observed ones are catalytically active: under resubmission to reaction conditions all complexes (namely acid **2**, zinc salt **10** and complex **8b**) proved active and provided the homoallylic alcohol product with 86–88% conversion and close to perfect selectivity (96% ee).

These findings, in combination with the fact that educt complexes involving a mono-zinc phosphate complex are energetically significantly higher in energy (see supporting information, chapter 3.9.2), render a dinuclear catalytic species with respect to zinc the most likely one. All experimental data as well as the theoretical results point to complex **8** to be the product of the treatment of **2** with reagent **4/9** (see Scheme 1b). It results from a quench of the first reagent equivalent by the acidic proton of TRIP (**2**) and the subsequent coordination of a second equivalent to the chiral zinc phosphate salt.

Nonetheless, our computational efforts support this hypothesis of a coordinated allyl-zinc species and the involvement of two zinc atoms in the active species, as the formation of such is thermodynamically and kinetically highly favored (see Scheme 1d). Note that the subscripts of ΔG and $\Delta\Delta\text{G}$ values give the point of reference (“ed” refers to educts; “ISR” stands for “infinitely separated reactants”).

Phosphoric acid **2** is quenched with zinc reagent **9** (formed by the zinc insertion into allylic bromide **3**) with a negligible barrier [$\Delta\text{G}_{\text{ISR}}^{\text{educt}} = -3.6$ kJ/mol; $\Delta\Delta\text{G}_{\text{ed}}^{\text{TS}} = +6.7$ kJ/mol; $\Delta\text{G}_{\text{ISR}}^{\text{Zn-salt}} = -85.3$ kJ/mol; obtained from RI-PBE²⁰⁻²¹-D3/def2²²-TZVPPD²²⁻²³+COSMO²⁴⁻²⁵ single point calculations]. Subsequently, the formed zinc salt can coordinate another equivalent of reagent **9**, leading to structures **B1** and **B1h**. Whereas **B1** represents the local minimum, the formation of the final educt complex **ed_{fav.}** requires severe geometrical rearrangements and thus **B1** is regarded as an off-cycle intermediate which leads to a non-productive pathway (see supporting information, chapter 3.9.1; pathways leading to the favored and disfavored enantiomers are labelled with the subfixes “fav.” and “dis.”, respectively). **B1h** however – which resembles assumed structure **8** (except the double coordination of the lactone carbonyl) – demonstrates a perfect starting point for the formation of **ed_{fav.}**: Following the reaction trajectory, the most likely subsequent event is the coordination of the aldehyde oxygen to the Lewis acidic zinc salt of **B1h** (see Figure 2: mechanistic cycle, **B1h** to **ed_{fav.}**). This weakens and finally breaks the coordination of the lactone-carbonyl group.

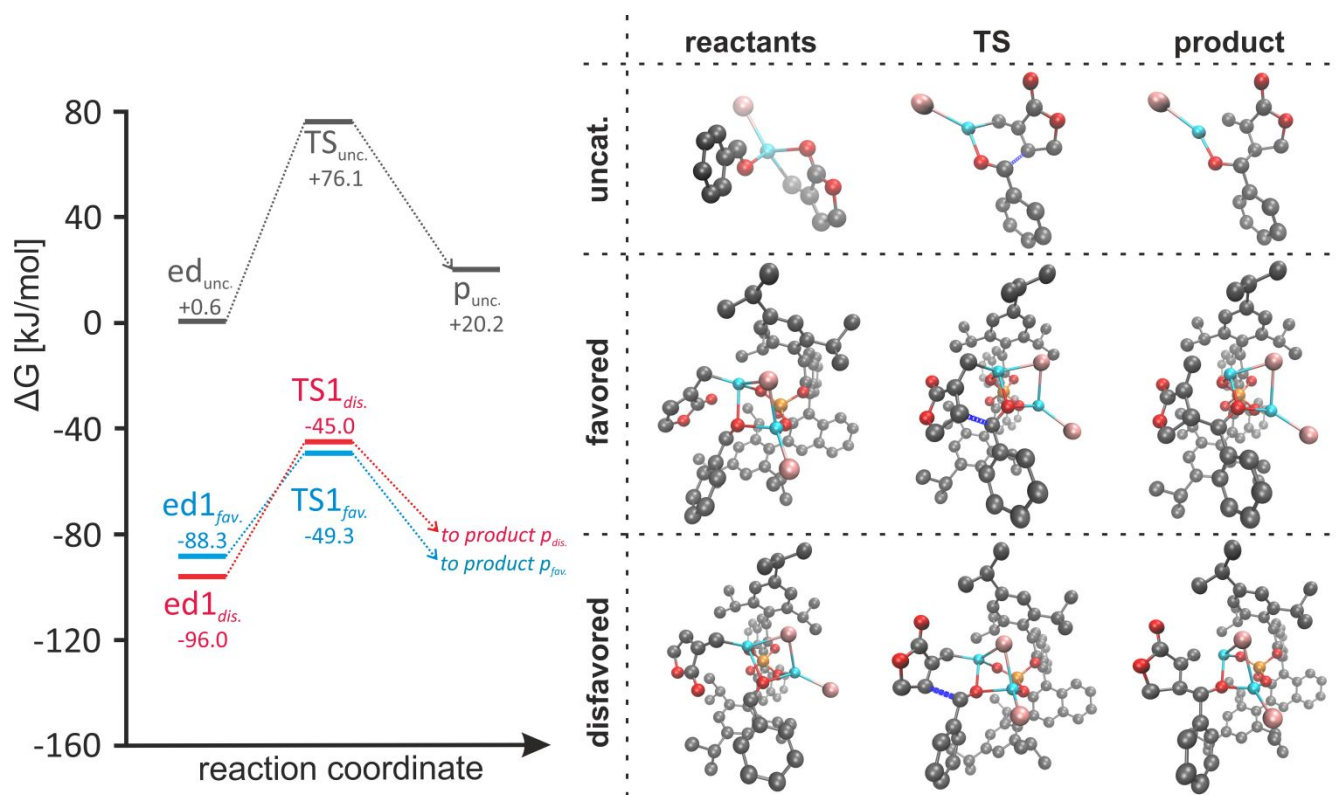


Figure 2. Left side: energy diagrams for the catalyzed and the uncatalyzed allylation step (■ blue = catalyzed reaction leading to the observed enantiomer; ■ red = catalyzed reaction leading to the non-observed enantiomer; ■ gray = uncatalyzed reaction); right side: reactants, products and transition state structures of the corresponding pathway (newly formed bond in the transition states is marked in dark blue).¹⁸ Only the energetically lowest pathways are shown, for all others see the supporting information. All presented data are given on the DLPNO-CCSD(T)/cc-pVTZ ΔG +COSMO level; the reference point (0 kJ/mol) represents the indefinitely separated reactants [the zinc salt of TRIP, reagent **9** and benzaldehyde (**5**)].

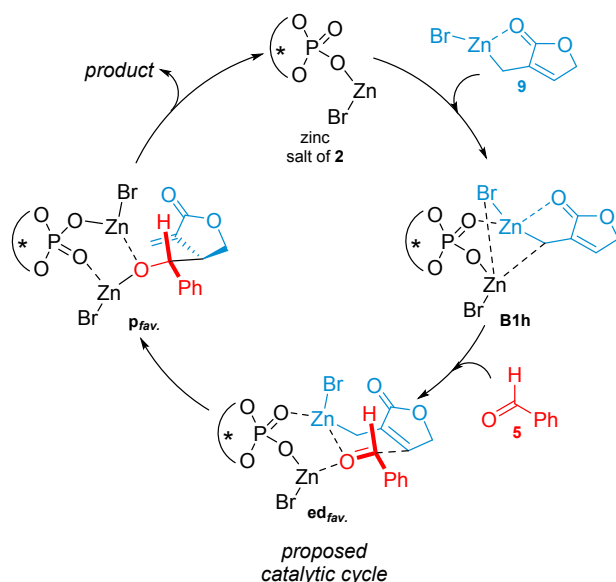


Figure 3. Mechanistic proposal of the catalytic cycle.

The obtained mono-coordination of the allylating reagent provides the possibility of an interaction of the aldehyde with both zinc atoms, increasing the aldehyde's polarization and translating to a more reactive electrophile

[see $\text{ed}_{\text{fav.}}$ and $\text{ed}_{\text{dis.}}$ in Figure 2 and 3; note that all calculated transition states with reasonable energies require this double coordination (for additional transition states see supporting information, chapter 3)].

The latter structures ($\text{ed}_{\text{fav.}}$ and $\text{ed}_{\text{dis.}}$) were originally computed from the coordination of the educt complex of the uncatalyzed reaction $\text{ed}_{\text{unc.}}$ to the zinc salt of the catalyst. Thus, they represent perfect starting points for the asymmetric catalysis.

Complex $\text{ed}_{\text{fav.}}$ readily transforms into the product complex $\text{p}_{\text{fav.}}$ via an energetic barrier of $\Delta\Delta G_{\text{ed}}^{\text{TS}} = +39.0$ kJ/mol (see Figure 2, left side). This compares to the lowest energy barrier for the formation of the experimentally disfavored enantiomer of $\Delta\Delta G_{\text{ed}}^{\text{TS}} = +51.0$ kJ/mol, giving a difference of 12.0 kJ/mol in favor of the experimentally observed results. This difference very well reflects the observed enantiomeric excess, which has been determined to be 94% at 4°C.¹¹

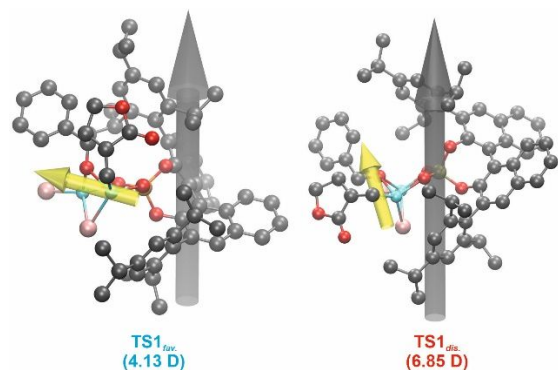


Figure 4. TS structures,¹⁸ overall dipole moment (gray arrow) and dipole moment of the lactone (yellow arrow); the overall dipole moment is given in brackets. All presented data are given on the DLPNO-CCSD(T)/cc-pVTZ level.

The rationale for the difference in the transition states may be found in the minimization of the dipole moment, especially with consideration of the apolar reaction medium (toluene). Whereas the favored TS_{fav} exhibits a dipole moment of 4.13 D, the disfavored TS_{dis} yields 6.85 D. This is reasoned by a different alignment of the lactone moiety and its dipole, which is positioned along the overall dipole moment in TS_{dis} . In contrast to structure TS_{dis} , the dipole moment of the lactone subunit is almost orthogonal to the overall dipole in TS_{fav} . (see Figure 4). Furthermore, the dipole moment of ed_{fav} was calculated to be 5.10 D, while the one of ed_{dis} was determined to be 4.74 D. Hence, for the favored pathway, the polarity of the complex decreases along the reaction coordinate towards the transition state, while for the disfavored pathway it increases significantly, reflecting in the complementary educt energies (ed_{dis} is slightly favored over ed_{fav} , see Figure 2). This adds to the energetic barriers and further favors the pathway of the observed stereoselectivity.

In addition, the experimental observation that allyl bromide leads to no detected stereoselection may be rationalized by this hypothesis, as allyl bromide exhibits a significantly lower dipole moment.

Moreover, the alignment of the aldehyde carbon and the β -carbon of the lactone forming the future C-C bond is much more favorable in structure ed_{fav} than in ed_{dis} , which can be attributed to unfavorable steric interactions with the isopropyl groups of the catalyst in the latter educt complex. Attempts to improve the alignment in ed_{dis} reverted to the original geometry when optimized. Hence, we conclude that the pathway leading to the experimentally disfavored enantiomer requires significantly more reorganization, contributing to the higher energetic barrier of TS_{dis} , additionally.

The uncatalyzed reaction is disfavored by 36.5 kJ/mol ($\Delta\Delta G_{\text{ed}}^{\text{TS}} = +75.5$ kJ/mol). Other coordination patterns of the educt complexes to the zinc salt of the TRIP catalyst yielded unfavorable pathways (see supporting information,

chapter 3.9.1). Important to note is that the catalysis provides the stereoselection, but the experimental data suggests, that the preceding in-situ formation of the allyl-zinc reagent demonstrates the rate determining step of the overall process, as at no time of the reaction the level of active zinc reagent exceeds the catalyst loading (see supporting information, chapter 2.3-2.4, for details).

Finally, the energies of the formed product complexes deserve some attention, as all reactions are endergonic (for energies of products see supporting information, chapter 3.8). This fact may reveal the role of the NH_4Cl additive, which has been either believed to activate the zinc dust or quench the obtained zinc alcoholate product yielding the free protonated alcohol and ZnX_2 (please note, that without the ammonium salt no reaction is observed regarding the catalyzed and the uncatalyzed reaction). With the reaction(s) being endergonic, the latter role of the additive seems to be supported by our calculations, as it provides the final pull the equilibrium to the product side. An alternative for this shift of the equilibrium would be a cluster formation of the zinc alcoholate product molecules, as described for Noyori's DAIB catalyzed, asymmetric alkylation of aldehydes with dialkylzinc reagents.²⁶ Nevertheless, the presence of the NH_4^+ proton and the significant bulk around the zinc-oxygen cluster favor the equilibrium push by the quenching scenario.

Conclusion

We have shown that the TRIP catalyzed asymmetric allylation via zinc reagents proceeds via the zinc salt of the chiral phosphoric acid. Addition of a second equivalent of the in situ formed reagent yields complex **Bih**, which – upon an approaching aldehyde – gives educt complex ed_{fav} , an ideal precursor for the final C-C bond formation. The catalysis is rationalized by the double coordination of the aldehyde oxygen by both Lewis acidic zinc atoms (see structure of TS_{fav}) and the required rigidity of the catalytic system stems from the Lewis basic interaction of the P=O oxygen to the allylzinc reagent. Perfectly aligned in ed_{fav} , the favorable enantiomer is formed via an energetic barrier of 39.0 kJ/mol ($\Delta\Delta G_{\text{ed}}^{\text{TS}}$). Thus, the formation of the experimentally non-observed enantiomer and the uncatalyzed reaction are outrun by 12.0 kJ/mol and 36.5 kJ/mol, respectively. The energetic difference in the transition states can be rationalized by the dipole moment of the corresponding complexes, which is minimized for the favored enantiomer. Important to note is the endergonic character of the final reaction step, which requires an external pull to the reaction system. This pull can be found in the protonic quench of the zinc alcoholate by the ammonium chloride additive. All these findings render a rather clear picture of the asymmetric catalysis in the case of this allylation process and provide another example for a counterion directed asymmetric catalytic process. Additionally, they may lead to a better

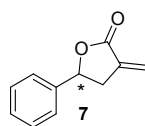
understanding of the Lewis acidic/basic interactions of this outstanding catalyst and stimulate new catalytic procedures of a similar type.

Experimentals

General. All chemicals were purchased from Sigma Aldrich or Acros Organics and were used as received, unless otherwise noted. All solvents were purchased from Roth, except Dioxane (Alfa Aasar) and dry toluene (Sigma Aldrich). Moisture sensitive reactions were performed using standard Schlenk techniques with argon 5.0. Analytical thin layer chromatography (TLC) was carried out on Merck TLC silica gel aluminum sheets (silica gel 60, F₂₅₄, 20 x 20 cm) and spots were visualized by UV light ($\lambda = 254$ nm) and by staining with cerium ammonium molybdate solution [50 g (NH₄)₆Mo₇O₂₄ were dissolved in 400 mL H₂O and 50 mL conc. H₂SO₄ was added followed by 2.0 g Ce(SO₄)₂ or KMnO₄ solution (1 g KMnO₄ and 2 g Na₂CO₃ were dissolved in 100 mL H₂O) and developed by heating with a heat gun. Column chromatography was performed on silica gel 60 from Merck with particle sizes 40–63 μ m. A 30- to 100-fold excess of silica gel was used with respect to the mass of dry crude product, depending on the separation problem. For sticky crude products, the crude material was dissolved in MeOH and subsequently adsorbed on the 2.5-fold excess of silica gel. Afterwards the solvent was removed in vacuum and the adsorbed crude material was dried in oil pump vacuum. The dimension of the column was adjusted to the required amount of silica gel and formed a pad between 20 and 40 cm of height. In general, the silica gel was mixed with the eluent and charged into the column before equilibration. Subsequently, the dissolved or adsorbed crude material was loaded onto the top of the silica gel and the mobile phase was forced through the column by pressure exerted by a rubber bulb pump.

Instrumentation. ¹H-, ¹³C-, and ³¹P-NMR spectra were recorded on a Bruker AVANCE III 300 spectrometer (¹H: 300.13 MHz; ¹³C: 75.47 MHz; ³¹P: 121.49 MHz) with an autosampler. Chemical shifts were referenced to the residual proton and carbon signal of the deuterated solvent [CDCl₃; $\delta = 7.26$ ppm (¹H), 77.16 ppm (¹³C)]. Chemical shifts δ are given in ppm (parts per million) and coupling constants *J* in Hz (Hertz). Deuterated solvents for nuclear resonance spectroscopy were purchased from Roth. Melting points were determined on a Gallenkamp MPD350.BM2.5 apparatus with an integrated microscopical support. They were measured in open capillary tubes with a mercury-in-glass thermometer and were not corrected. IR-spectra were recorded neat on a Bruker Alpha-P (ATR) instrument. The specific optical rotation was determined on a Perkin Elmer Polarimeter 341 with an integrated sodium vapor lamp. All samples were measured in CHCl₃ and CH₂Cl₂ (both were purchased from Sigma Aldrich, ACS spectrophotometric grade, $\geq 99.8\%$) at the D-line of the sodium light ($\lambda = 589$ nm) under non-tempered conditions between 22 °C and 27 °C. High resolution mass spectra were recorded on an Agilent 6230

TOF LC/MS using ESI (positive mode, capillary voltage 3.5 kV) or APCI (negative mode, 5.0 kV) methods. Chiral HPLC analysis was performed on a Shimadzu HPLC system [DGPU-20A (degasser), LC-20A (pump), SIL-20A (autosampler), CTO-20AC (column oven), SPD-M20A (detector), CBM-20AC (controller)] with *n*-heptane/2-PrOH as eluent using Daicel columns [dimension: 4.6 x 250 mm, 5 μ m particle size, except Chiralpak AD (10 μ m) and Chiralcel OJ (10 μ m)] and conditions as specified below. All GC-MS measurements were carried out with an Agilent 7890A GC system, equipped with an Agilent 5975C mass-selective detector (electron impact, 70 eV), a HP-5-MS column (30m x 0.25 mm x 0.25 μ m film) and an Agilent 7697A headspace autosampler using He as carrier gas at a flow of 0.7 mL/min. The following temperature program was used in all GC-MS headspace measurements: initial temperature 40°C, hold for 5 min, 10 °C/min, to 200 °C. Headspace parameters: vial pressurization gas: He; loop size: 1 mL; transfer line: DB-ProSteel (0.53 mm diameter); oven temperature: 50°C; loop temperature: 55°C; transfer line: 60°C; vial equilibration time: 4 min; Injection duration: 0.5 min; vial size: 20 mL; vial shaking: level 5, 71 shakes per min with acceleration of 260 cm/s²; fill pressure: 15 psi.



3-Methylene-5-phenyldihydrofuran-

2(3H)-one (7). A 5 mL screw cap vial with magnetic stirring bar was charged with zinc (33.0 mg, 500 μ mol, 5 eq.), ammonium chloride (43.0 mg, 800 μ mol, 8 eq.) and (*S*)-

3,3'-bis(2,4,6-triisopropylphenyl)-1,1'-binaphthyl-2,2'-diyl hydrogenphosphate (TRIP, 7.5 mg, 10.0 μ mol, 0.1 eq.) followed by toluene (1.0 mL), benzaldehyde (10.6 mg, 100 μ mol) and allyl bromide 4 (29.0 mg, 150 μ mol, 1.5 eq.). The mixture was stirred (720 rpm) at room temperature for 16 h and was consecutively quenched by the addition of saturated aqueous NH₄Cl solution (5 mL). The mixture was extracted with EtOAc (3 x 10 mL) and the combined organic phase was dried over Na₂SO₄, filtered and concentrated under reduced pressure. The obtained crude product [mixture of compound 6 (free alcohol) and 7 (lactone)] was dissolved in CH₂Cl₂ and *para*-toluenesulfonic acid hydrate (4 mg, 20 μ mol, 20 mol-%) was added. The reaction mixture was stirred for 16 h, quenched with NaHCO₃ aqueous solution (saturated) and extracted with CH₂Cl₂ (3 x 10 mL). The combined organic phase was dried over Na₂SO₄, filtered and concentrated. The crude product was purified via flash chromatography (SiO₂, hexanes/EtOAc 5/1) to give product 7 (20 mg, 60 μ mol, 60%) as a colorless oil.

$[\alpha]_D^{20} = +4.4$ (*c* = 2.0, CHCl₃); ¹H-NMR (300.13 MHz, CDCl₃): 7.46 – 7.28 (m, 5H), 6.31 (t, *J* = 2.8 Hz, 1H), 5.69 (t, *J* = 2.5 Hz, 1H), 5.53 (dd, *J*₁ = 7.9, *J*₂ = 6.6 Hz, 1H), 3.41 (ddt, *J*₁ = 17.1, *J*₂ = 8.1, *J*₃ = 2.5 Hz, 1H), 2.91 (ddt, *J*₁ = 17.1, *J*₂ = 6.4, *J*₃ = 2.9 Hz, 1H); ¹³C{¹H}-NMR (75.47 MHz, CDCl₃): 170.3, 139.9, 134.3, 129.0, 128.7, 125.5, 122.6, 78.1, 36.4; IR (film) $\tilde{\nu} = 3093, 3066, 3050, 3037, 2974, 2919, 2853, 1752, 1602, 1551, 1496, 1459, 1437, 1402, 1375, 1319, 1277, 1240, 1215, 1126, 1080,$

1020, 985, 962, 938, 818, 761, 701, 639, 562 cm⁻¹; HPLC analysis on chiral stationary phase {Daicel Chiralpak OD-H, *n*-heptane/2-propanol 90/10, 1.0 mL/min, 30 °C, UV 215 nm, *t*_{ret}(enantiomer 1) = 8.7 min, *t*_{ret}(enantiomer 2) = 9.8 min}; *t*_{ret}(major isomer) = 8.7 min, 28% ee; HRMS(ESI): *m/z*: calc. for C₁₁H₁₁O₂⁺: 175.0754 [M+H]⁺, found: 175.0755.

General procedure for the preparation of racemic reference material. A HPLC vial with magnetic stirring bar was charged with the ketone or aldehyde (25.0 μmol, 1 eq.), zinc (8.0 mg, 125 μmol, 5 eq.), NH₄Cl (11.0 mg, 200 μmol, 8 eq.) and diphenyl phosphate (2.0 mg, 8.0 μmol, 0.3 eq.). Allylic bromide **4** (36.0 μmol, 1.5 eq.) dissolved in toluene (200 μL) was added and the reaction mixture was stirred at room temperature for 16 h. The suspension was filtered through a plug of silica gel (~1 g), the plug was rinsed with additional EtOAc (ca. 1 mL) and the combined filtrates were concentrated. The residue was dissolved in a small amount of EtOAc (ca. 100 μL) and half of the solution was adsorbed on the starting line of a silica gel TLC plate (~8 cm wide). The plate was developed in the solvent indicated for flash chromatography for the specific compound (indicated below) and the product band was scratched off. The obtained silica gel with the adsorbed product was transferred into a HPLC vial with magnetic stirring bar and was extracted by stirring with 2-propanol (800 μL) for 30 min at 22 °C. The suspension was filtered through a syringe filter (Nylon, 0.2 μm) and subjected to HPLC-MS and HPLC-UV analysis on a chiral stationary phase.

Mechanistic Studies

General. All reactions were performed in dry and degassed CDCl₃. All samples were prepared under a dry argon atmosphere in flame-dried glass ware. ³¹P-NMR spectra were referenced to dimethyl methylphosphonate (δ = +33.8 ppm) unless otherwise noted. The reference was filled into a small capillary (50 μL volume), which was sealed by flame and added to the corresponding sample to avoid interaction of the standard with the reaction mixture. ¹H- and ¹³C-spectra were referenced to the residual solvent peak of CDCl₃ [δ = 7.26 ppm (¹H) and 77.16 ppm (¹³C)].



TRIP (2) spectra in the presence of allylic zinc reagent derived from 4. (*S*)-TRIP [(*S*)-**2**, 22.5 mg, 30.0 μmol), zinc (98.1 mg,

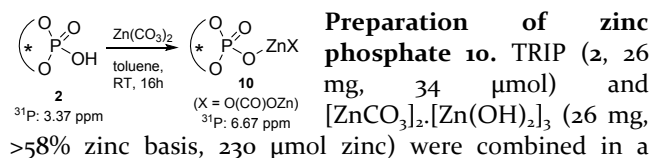
1.50 mmol, 50 eq.) and ammonium chloride (128 mg, 2.40 mmol, 80 eq.) were combined in a Schlenk tube with magnetic stirring bar and suspended in CDCl₃ (600 μL). **4** (29.0 mg, 150 μmol, 21.0 μL, 5 eq.) was added and the reaction mixture was stirred for 1 h. The reaction mixture was filtered through a syringe filter (PVDF, 0.45 μm, 33 mm diameter) and the filtrate was filled into a NMR tube and analysed. After ¹H-, ¹³C- and a NOESY spectra were recorded, the capillary with dimethyl methylphosphonate

was added to reference the ³¹P-NMR, which was recorded subsequently.

Time study of the zinc insertion reaction forming reagent 9. Zinc dust (10.1 mg, 155 μmol, 5 eq.) and ammonium chloride (13.3 mg, 248 μmol, 8 eq.) were combined in a 1 mL HPLC vial. A stock solution (200 μL toluene and 50 μL 2-ⁱPr₂O) containing the bromolactone **3** (6.5 mg, 37 μmol, 1.2 equiv.) was added and the reaction mixture was stirred at room temperature. Samples of 50 μL were withdrawn after the times given below, applied to a syringe with filter, diluted with 500 μL of toluene and filtered. The filtrate was quenched with aqueous HCl (1 M, 100 μL), the phases were separated, the organic phase was dried over Na₂SO₄ and subjected to GC-FID analysis [for conditions and instrumentation see general part; *t*_{ret}(quenched **9**) = 6.65 min, *t*_{ret}(**3**) = 11.20 min].

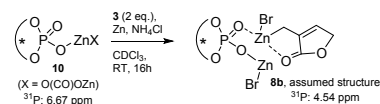
Time study of the catalytic reaction with regard to the accumulation of 9 over time. Zinc dust (10.1 mg, 155 μmol, 5 eq.) and ammonium chloride (13.3 mg, 248 μmol, 8 eq.) were combined in a 1 mL HPLC vial. A stock solution (200 μL toluene and 50 μL 2-ⁱPr₂O) containing the bromolactone **3** (6.5 mg, 37 μmol, 1.2 equiv.), benzaldehyde (**5**, 3.3 mg, 31 μmol, 1 eq.) and (*R*)-TRIP (**2**, 2.3 mg, 3.1 μmol, 0.1 eq., 10 mol-%) was added and the reaction mixture was stirred at room temperature. Samples of 50 μL were withdrawn after the times given below, applied to a syringe with filter, diluted with 500 μL of toluene and filtered. The filtrate was quenched with aqueous HCl (1 M, 100 μL), the phases were separated, the organic phase was dried over Na₂SO₄ and subjected to GC-FID analysis [for conditions and instrumentation see general part; *t*_{ret}(quenched **9**) = 6.65 min, *t*_{ret}(**3**) = 11.20 min, *t*_{ret}(**SI01**) = 18.41 min]. The final sample (after 23 h reaction time) was dried by a positive stream of air, redissolved in 2-PrOH (500 μL) and subjected to HPLC-UV analysis on a chiral stationary phase {Daicel Chiralpak AD, *n*-heptane/2-propanol 85/15, 0.7 mL/min, 18 °C, UV 215 nm, *t*_{ret}(enantiomer 1) = 13.0 min, *t*_{ret}(enantiomer 2) = 14.1 min}; *t*_{ret}(major isomer) = 13.7 min, 92% ee.

GC-MS headspace measurements for the indirect detection of the zinc phosphate salt of 2. Zinc dust (33 mg, 500 μmol) ammonium chloride (43 mg, 800 μmol) and TRIP (**2**, 22.5 mg, 30 μmol) and a magnetic stirring bar were placed into an agilent headspace vial. The vial was capped and crimped, evacuated and refilled with dry N₂. A solution of **4** (29 mg, 150 μmol, 21 μL) in dry dichloromethane (200 μL) was added. The reaction mixture was stirred at room temperature for 3 h and subjected directly to the GC-MS headspace sampling under the conditions outlined in the general section. *t*_{ret}(quenched reagent **9**) = 6.03 min.



Preparation of zinc phosphate 10. TRIP (**2**, 26 mg, 34 μmol) and [ZnCO₃]₂·[Zn(OH)₂]₃ (26 mg, >58% zinc basis, 230 μmol zinc) were combined in a

Schlenk tube and dry, degassed CDCl_3 (700 μL) was added. The slurry was stirred for 16 h at room temperature, and transferred via syringe, canula and syringe filter (PVDF, 0.45 μm , 33 mm diameter) into a NMR tube under argon protective gas atmosphere. A capillary with dimethyl methylphosphonate was added to reference the ^{31}P -NMR and the tube was capped and subjected to NMR analysis. After the analysis, 70 μL were withdrawn from the sample in order to test its catalytic activity. The remaining 630 μL were directly subjected to the next reaction step. ^1H -NMR (CDCl_3 , 300 MHz): δ = 7.87 (d, J = 8.2, 2H), 7.46 (ddd, J_1 = 8.1, J_2 = 6.3, J_3 1.5 Hz, 2H), 7.33 – 7.20 (m, 4H), 7.01 (d, J = 1.7 Hz, 2H), 6.94 (d, J = 1.7 Hz, 2H), 2.88 (p, J = 6.9 Hz, 2H), 2.66 (tt, J_1 = 13.5, J_2 = 6.8 Hz, 4H), 1.26 (d, J = 4.5 Hz, 6H), 1.23 (d, J = 4.4 Hz, 6H), 1.07 (d, J = 6.8 Hz, 6H), 0.97 (d, J = 6.7 Hz, 6H), 0.91 (d, J = 6.8 Hz, 6H), 0.79 (d, J = 6.7 Hz, 6H); $^{13}\text{C}\{^1\text{H}\}$ -NMR (CDCl_3 , 75 MHz): δ = 148.6, 148.5, 147.9, 146.8, 146.6, 132.7, 132.5, 132.3, 132.2, 130.8, 128.2, 127.3, 126.2, 125.4, 122.3, 121.0, 120.3, 34.3, 31.0, 30.8, 26.3, 25.1, 24.3, 24.1, 23.4, 23.3; $^{31}\text{P}\{^1\text{H}\}$ -NMR (CDCl_3 , 121.5 MHz): δ = 6.67.



Preparation of complex **8b** from zinc phosphate **10**.

Zinc dust (10 mg, 153 μmol , 5 eq.) and ammonium chloride (13 mg, 243 μmol , 8 eq.) were combined in a flame dried Schlenk tube. The solution containing zinc phosphate **10** in CDCl_3 (ca. 630 μL) was added, followed by bromolactone **3** (6.8 μL , 11.6 mg, 66 μmol) and the reaction mixture was stirred for 16 h at room temperature. Subsequently, it was transferred via syringe, canula and syringe filter (PVDF, 0.45 μm , 33 mm diameter) into a NMR tube under argon protective gas atmosphere. A capillary with dimethyl methylphosphonate was added to reference the ^{31}P -NMR and the tube was capped and subjected to NMR analysis. As the solubility of the complex proved low, 100 μL of DMSO- d_6 were added and the NMR analysis was repeated. Subsequently, 70 μL of this reaction mixture were used to test the catalytic potential of complex **8b** as described below.

Testing the catalytic activity of salt **10 and complex **8b**.** Zinc dust (10 mg, 153 μmol , 5 eq.) and ammonium chloride (13 mg, 243 μmol , 8 eq.) were combined in a flame dried Schlenk tube. Dry toluene (1 mL) was added, followed by the catalyst preparation (3.4 μmol in 70 μL CDCl_3), benzaldehyde (**5**, 3.0 μL , 2.9 mg, 30 μmol) and bromolactone **3** (3.5 μL , 5.8 mg, 33 μmol). The remaining slurry was stirred for 16 h at room temperature, filtered through a pad of silica and concentrated to dryness. The residue was dissolved in 2-PrOH and subjected to HPLC-UV analysis on a chiral stationary phase {Daicel Chiralpak IA, *n*-heptane/2-PrOH 95/5, 1.0 mL/min, 30°C, UV 215 nm, t_{ret} (enantiomer 1) = 26.4 min, t_{ret} (enantiomer 2) = 28.3}; t_{ret} (major isomer) = 28.7 min (catalyst **2**), 28.7 min (catalyst **10**), 28.7 min (catalyst **8b**); ee = 96% for all catalysts. All other physical data has been reported previously.¹¹

Computational Methods.

Conformational searches of the catalyst and the substrates were performed with the COSMO-conf program²⁷ at the BP86²⁸⁻²⁹/def-SVP²²⁻²³ level and single points were calculated at the BP86/def-TZVP level. All calculations were run with the TURBOMOLE program (version 6.6),³⁰ while the DLPNO-CCSD(T)/cc-pVTZ calculations were performed with ORCA 4.0.1.2.³¹ The geometries were optimized using the PBE functional,²⁰⁻²¹ the def2-SVP basis set and D3-dispersion correction. To reduce computational cost, the RI-approximation was utilized. To model solvent effects, the geometries were reoptimized at the RI-PBE-D3/def2-SVP level employing the COSMO-solvation model for toluene (ϵ_r = 2.438 at 0 °C).²⁴⁻²⁵ Transition states were located by using TURBOMOLE's woelfling-program³² followed by subsequent geometry optimization. Analytical normal modes were determined using TURBOMOLE's aoforce-program for confirmation of the stationary points and transition state search. After scaling of the frequencies³³ the rigid-rotor-harmonic-oscillator (RRHO) approximation was used to calculate zero point vibrational energies and thermal properties (at 4 °C). Single points of the transition states and minima were calculated with RI-PBE-D3/def2-TZVPPD (with and without computing solvation effects), B3LYP-D3/def2-TZVPPD and DLPNO-CCSD(T)/cc-pVTZ (without solvation effects). Zero-point energies and thermal corrections for the COSMO-reoptimized structures and the single point calculations were taken from the RI-PBE-D3/def2-SVP gas phase calculations. COSMO corrected energies for the B3LYP^{28, 34-35}-D3/def2-TZVPPD and DLPNO-CCSD(T)³⁶/cc-pVTZ³⁷⁻³⁸ were obtained from the RI-PBE-D3/def2-TZVPPD single point calculations. All presented data are given on the DLPNO-CCSD(T)/cc-pVTZ ΔG +COSMO level unless otherwise noted.

ASSOCIATED CONTENT

Supporting Information

The Supporting Information is available free of charge on the ACS Publications website.

NMR- and HPLC spectra, and additional data to the performed calculations (PDF)

Coordinates of calculated structures (PDF)

AUTHOR INFORMATION

Corresponding Author

* Michael Fuchs, University of Graz, Institute of Chemistry, Bioorganic and Organic Chemistry, Heinrichstrasse 28/II, 8010 Graz, Austria, Europe; mail to: michael.fuchs@uni-graz.at.

* A. Daniel Boese, University of Graz, Institute of Chemistry, Physical and Theoretical Chemistry, Heinrichstrasse 28/IV, 8010 Graz, Austria, Europe; mail to: adrian.daniel.boese@uni-graz.at.

ACKNOWLEDGMENT

M. Lazzarotto and M. Fuchs are grateful for a grant of the Austrian Science Fund (FWF, P 31276-B21). K. Faber, K. Zangger, B. Werner, E. Schwarz, J. Schachner and R. Fischer are acknowledged for fruitful discussion. J. Goodman, J. Antilla, K. N. Houk and M. Grayson are acknowledged for discussion of the content prior to submission.

REFERENCES

- (1) Cheong, P. H.-Y.; Legault, C. Y.; Um, J. M.; Çelebi-Ölçüm, N.; Houk, K. N., Quantum Mechanical Investigations of Organocatalysis: Mechanisms, Reactivities, and Selectivities. *Chem. Rev.* **2011**, *111*, 5042-5137.
- (2) Sunoj, R. B., Proline-derived organocatalysis and synergism between theory and experiments. *WIREs Comput. Mol. Sci.* **2011**, *1*, 920-931.
- (3) Sunoj, R. B., Transition State Models for Understanding the Origin of Chiral Induction in Asymmetric Catalysis. *Acc. Chem. Res.* **2016**, *49*, 1019-1028.
- (4) Allemann, C.; Gordillo, R.; Clemente, F. R.; Cheong, P. H.-Y.; Houk, K. N., Theory of Asymmetric Organocatalysis of Aldol and Related Reactions: Rationalizations and Predictions. *Acc. Chem. Res.* **2004**, *37*, 558-569.
- (5) Ramachandran, P. V.; Gagare, P. D.; Nicponski, D. R., 2.01 Allylborons. In *Comprehensive Organic Synthesis II (Second Edition)*, Knochel, P., Ed. Elsevier: Amsterdam, 2014; pp 1-71.
- (6) Kim, S. W.; Zhang, W.; Krische, M. J., Catalytic Enantioselective Carbonyl Allylation and Propargylation via Alcohol-Mediated Hydrogen Transfer: Merging the Chemistry of Grignard and Sabatier. *Acc. Chem. Res.* **2017**, *50*, 2371-2380.
- (7) Denmark, S. E.; Fu, J., Catalytic Enantioselective Addition of Allylic Organometallic Reagents to Aldehydes and Ketones. *Chem. Rev.* **2003**, *103*, 2763-2793.
- (8) Lachance, H.; Hall, D. G., Allylboration of Carbonyl Compounds. *Org. React.* **2008**, *73*, 1-573.
- (9) Yamamoto, H.; Wadamoto, M., Silver-Catalyzed Asymmetric Allylation: Allyltrimethoxysilane as a Remarkable Reagent. *Chem. Asian J.* **2007**, *2*, 692-698.
- (10) Yus, M.; González-Gómez, J. C.; Foubelo, F., Catalytic Enantioselective Allylation of Carbonyl Compounds and Imines. *Chem. Rev.* **2011**, *111*, 7774-7854.
- (11) Fuchs, M.; Schober, M.; Orthaber, A.; Faber, K., Asymmetric Synthesis of β -Substituted α -Methylenebutyrolactones via TRIP-Catalyzed Allylation: Mechanistic Studies and Application to the Synthesis of (S)-(-)-Hydroxymatairesinol. *Adv. Synth. Catal.* **2013**, *355*, 2499-2505.
- (12) Hartmann, P.; Lazzarotto, M.; Steiner, L.; Cigan, E.; Poschenrieder, S.; Sagmeister, P.; Fuchs, M., TRIP-Catalyzed Asymmetric Synthesis of (+)-Yatein, (-)- α -Conidendrin, (+)-Isostegane, and (+)-Neoisostegane. *J. Org. Chem.* **2019**, *84*, 5831-5837.
- (13) Hoffmann, S.; Seayad, A. M.; List, B., A Powerful Brønsted Acid Catalyst for the Organocatalytic Asymmetric Transfer Hydrogenation of Imines. *Angew. Chem. Int. Ed.* **2005**, *44*, 7424-7427.
- (14) Jain, P.; Antilla, J. C., Chiral Brønsted Acid-Catalyzed Allylboration of Aldehydes. *J. Am. Chem. Soc.* **2010**, *132*, 11884-11886.
- (15) Grayson, M. N.; Pellegrinet, S. C.; Goodman, J. M., Mechanistic Insights into the BINOL-Derived Phosphoric Acid-Catalyzed Asymmetric Allylboration of Aldehydes. *J. Am. Chem. Soc.* **2012**, *134*, 2716-2722.
- (16) Rodríguez, E.; Grayson, M. N.; Asensio, A.; Barrio, P.; Houk, K. N.; Fustero, S., Chiral Brønsted Acid-Catalyzed Asymmetric Allyl(propargyl)boration Reaction of ortho-Alkynyl Benzaldehydes: Synthetic Applications and Factors Governing the Enantioselectivity. *ACS Catal.* **2016**, *6*, 2506-2514.
- (17) Wang, H.; Jain, P.; Antilla, J. C.; Houk, K. N., Origins of Stereoselectivities in Chiral Phosphoric Acid Catalyzed Allylboration and Propargylations of Aldehydes. *J. Org. Chem.* **2013**, *78*, 1208-1215.
- (18) Humphrey, W.; Dalke, A.; Schulten, K., VMD: Visual molecular dynamics. *J. Mol. Graphics* **1996**, *14*, 33-38.
- (19) Lacasse, M.-C.; Poulard, C.; Charette, A. B., Iodomethylzinc Phosphates: Powerful Reagents for the Cyclopropanation of Alkenes. *J. Am. Chem. Soc.* **2005**, *127*, 12440-12441.
- (20) Perdew, J. P.; Burke, K.; Ernzerhof, M., Generalized Gradient Approximation Made Simple. *Phys. Rev. Lett.* **1996**, *77*, 3865-3868.
- (21) Perdew, J. P.; Burke, K.; Ernzerhof, M., Generalized Gradient Approximation Made Simple [Phys. Rev. Lett. 77, 3865 (1996)]. *Phys. Rev. Lett.* **1997**, *78*, 1396-1396.
- (22) Weigend, F., Accurate Coulomb-fitting basis sets for H to Rn. *Phys. Chem. Chem. Phys.* **2006**, *8*, 1057-1065.
- (23) Weigend, F.; Ahlrichs, R., Balanced basis sets of split valence, triple zeta valence and quadruple zeta valence quality for H to Rn: Design and assessment of accuracy. *Phys. Chem. Chem. Phys.* **2005**, *7*, 3297-3305.
- (24) Klamt, A.; Moya, C.; Palomar, J., A Comprehensive Comparison of the IEFPCM and SS(V)PE Continuum Solvation Methods with the COSMO Approach. *J. Chem. Theory Comput.* **2015**, *11*, 4220-4225.
- (25) Klamt, A.; Schüürmann, G., COSMO: a new approach to dielectric screening in solvents with explicit expressions for the screening energy and its gradient. *J. Chem. Soc., Perkin Trans. 2* **1993**, 799-805.
- (26) Noyori, R.; Kitamura, M., Enantioselective Addition of Organometallic Reagents to Carbonyl Compounds: Chirality Transfer, Multiplication, and Amplification. *Angew. Chem. Int. Ed.* **1991**, *30*, 49-69.
- (27) COSMOconf 4.1, COSMOlogic GmbH & Co KG, <http://www.cosmologic.de>.
- (28) Becke, A. D., Density-functional exchange-energy approximation with correct asymptotic behavior. *Phys. Rev. A* **1988**, *38*, 3098-3100.
- (29) Perdew, J. P., Density-functional approximation for the correlation energy of the inhomogeneous electron gas. *Phys. Rev. B* **1986**, *33*, 8822-8824.
- (30) TURBOMOLE 6.6 2015, a development of the University of Karlsruhe and Forschungszentrum Karlsruhe GmbH, 1989-2007, TURBOMOLE GmbH, since 2007; available from <http://www.turbomole.com>
- (31) Frank, N., Software update: the ORCA program system, version 4.0. *WIREs Comput. Mol. Sci.* **2018**, *8*:e1327.
- (32) Plessow, P., Reaction Path Optimization without NEB Springs or Interpolation Algorithms. *J. Chem. Theory Comput.* **2013**, *9*, 1305-1310.
- (33) Kesharwani, M. K.; Brauer, B.; Martin, J. M. L., Frequency and Zero-Point Vibrational Energy Scale Factors for Double-Hybrid Density Functionals (and Other Selected Methods): Can Anharmonic Force Fields Be Avoided? *J. Phys. Chem. A* **2015**, *119*, 1701-1714.
- (34) Becke, A. D., Density-functional thermochemistry. III. The role of exact exchange. *J. Chem. Phys.* **1993**, *98*, 5648-5652.
- (35) Lee, C.; Yang, W.; Parr, R. G., Development of the Colle-Salvetti correlation-energy formula into a functional of the electron density. *Phys. Rev. B* **1988**, *37*, 785-789.
- (36) Neese, F.; Hansen, A.; Liakos, D. G., Efficient and accurate approximations to the local coupled cluster singles doubles method using a truncated pair natural orbital basis. *J. Chem. Phys.* **2009**, *131*, 064103.

1 (37) Dunning, T. H., A Road Map for the Calculation of
2 Molecular Binding Energies. *J. Phys. Chem. A* **2000**, *104*, 9062-
3 9080.

4 (38) Kendall, R. A.; Jr., T. H. D.; Harrison, R. J., Electron affinities
5 of the first-row atoms revisited. Systematic basis sets and wave
6 functions. *J. Chem. Phys.* **1992**, *96*, 6796-6806.

7
8
9
10
11
12
13
14
15
16
17
18
19
20
21
22
23
24
25
26
27
28
29
30
31
32
33
34
35
36
37
38
39
40
41
42
43
44
45
46
47
48
49
50
51
52
53
54
55
56
57
58
59
60

TOC Graph

